Laser ultrasonic surface wave dispersion technique for non-destructive evaluation of human dental enamel

Hsiao-Chuan Wang[1*], Simon Fleming[1], Yung-Chun Lee[2], Sue Law[1], Michael Swain[3], and Jing Xue[3, 4]

[1]*Institue of Photonics and Optical Science, School of Physics, University of Sydney, NSW 2006, Australia*
[2]*Department of Mechanical Engineering, National Cheng Kung University, Tainan City, Taiwan*
[3]*Faculty of Dentistry, University of Sydney, NSW 2006, Australia*
[4]*State Key Laboratory of Oral Diseases, Sichuan University, Chengdu, 610041, P. R. China*
david.wang@usyd.edu.au

Abstract: This paper describes a novel optical system for clinical diagnosis of dental enamel based on its elasticity. Current examination techniques are typically destructive, and frequently impractical for *in-vivo* inspection. This paper describes the first application of a laser ultrasonic non-destructive evaluation (NDE) method for clinical dental diagnosis. It performs remote elasticity evaluation on small dimension samples. A focused laser line-source generates broadband surface acoustic wave (SAW) impulses which are detected with a simplified optical fibre interferometer. The measured SAW velocity dispersion spectrum was in turn used to characterise the elasticity of the specimen. Different metal structures were measured to verify the system performance. The results agree well with theoretical values and confirm the reliability and accuracy of the laser NDE system. This technique was then applied to evaluate the surface of sound natural human dental enamel. The measured dispersion spectra match theoretical expectations and the influences of both the enamel and the underlying dentin on the surface wave propagation were observed. This is the first time, to the best of our knowledge, that a laser based SAW velocity dispersion technique has been successfully applied on human dental enamel. As a remote, non-destructive technique it is applicable in-vivo and opens the way for early diagnosis of dental caries.

OCIS codes: 120.3890 (Medical optics instrumentation); 120.4290 (Nondestructive testing); 280.3375 (Laser induced ultrasonics); 240.6690 (Surface waves); 120.0280 (Remote sensing and sensors); 060.2370 (Fibre optics sensors).

References and links

1. W. D. Miller, "*Agency of micro-organisms in decay of the teeth*", Dental Cosmos, 1883.
2. B. Krasse, "Biological factors as indicators of future caries," Int. Dent. J. **38**(4), 219–225 (1988).
3. F. Feagin, T. Koulourides, and W. Pigman, "The characterization of enamel surface demineralization, remineralization, and associated hardness changes in human and bovine material," Arch. Oral Biol. **14**(12), 1407–1417 (1969).
4. S. Habelitz, S. J. Marshall, G. W. Marshall, Jr., and M. Balooch, "Mechanical properties of human dental enamel on the nanometre scale," Arch. Oral Biol. **46**(2), 173–183 (2001).
5. J. L. Cuy, A. B. Mann, K. J. Livi, M. F. Teaford, and T. P. Weihs, "Nanoindentation mapping of the mechanical properties of human molar tooth enamel," Arch. Oral Biol. **47**(4), 281–291 (2002).
6. A. I. Ismail, "Visual and visuo-tactile detection of dental caries," J. Dent. Res. **83** (1), C56–C66 (2004).
7. F. Lippert, D. M. Parker, and K. D. Jandt, "In vitro demineralization/remineralization cycles at human tooth enamel surfaces investigated by AFM and nanoindentation," J. Colloid Interface Sci. **280**(2), 442–448 (2004).
8. T. Kundu, ed., *Ultrasonic nondestructive evaluation: engineering and biological material characterization*. 2004, CRC Press.
9. D. Schneider, B. Schultrich, H. J. Scheibe, H. Ziegele, and M. Griepentrog, "A laser-acoustic method for testing and classifying hard surface layers," Thin Solid Films **332**(1–2), 157–163 (1998).

#111936 - $15.00 USD Received 9 Jun 2009; revised 28 Jul 2009; accepted 29 Jul 2009; published 19 Aug 2009

10. C. Glorieux, W. Gao, S. E. Kruger, K. Van de Rostyne, W. Lauriks, and J. Thoen, "Surface acoustic wave depth profiling of elastically inhomogeneous materials," J. Appl. Phys. **88**(7), 4394–4400 (2000).
11. J. A. Rogers, A. A. Maznev, M. J. Banet, and K. A. Nelson, "Optical Generation and Characterization of Acoustic Waves in Thin Films: Fundamentals and Applications," Annu. Rev. Mater. Sci. **30**(1), 117–157 (2000).
12. Y. C. Lee, J. O. Kim, and J. D. Achenbach, "*Measurement of elastic constants and mass density by acoustic microscopy*", IEEE Ultrasonics Symposium, vol.**1**, pp.607–612, October 1993.
13. C. S. Scruby, and L. E. Drain, *Laser Ultrasonics: Techniques and Applications*. 1990: Adam Hilger Ltd.
14. A. Neubrand, and P. Hess, "Laser generation and detection of surface acoustic waves: Elastic properties of surface layers," J. Appl. Phys. **71**(1), 227–238 (1991).
15. J. Monchalin, "Optical Detection of Ultrasound," IEEE Trans. Ultrason. Ferroelectr. Freq. Control **UFFC-33**(5), 485–499 (1986).
16. R. J. Dewhurst, and Q. Shan, "Optical remote measurement of ultrasound," Meas. Sci. Technol. **10**(11), R139–R168 (1999).
17. B. Mitra, A. Shelamoff, and D. J. Booth, "An optical fibre interferometer for remote detection of laser generated ultrasonics," Meas. Sci. Technol. **9**(9), 1432–1436 (1998).
18. A. J. A. Bruinsma, and J. A. Vogel, "Ultrasonic noncontact inspection system with optical fiber methods," Appl. Opt. **27**(22), 4690–4695 (1988).
19. T. D. Dudderar, C. P. Burger, J. A. Gilbert, J. A. Smith, and B. R. Peters, "Fiber optic sensing for ultrasonic NDE," J. Nondestructive Evaluation **6**(3), 135–146 (1987).
20. H. S. Park, G. Thursby, and B. Culshaw, "Detection of laser-generated ultrasound based on phase demodulation technique using a fibre Fabry-Perot interferometer," Meas. Sci. Technol. **16**(6), 1261–1266 (2005).
21. T. S. Jang, S. S. Lee, I. B. Kwon, W. J. Lee, J. J. Lee, T. S. Jang, S. S. Lee, I. B. Kwon, W. J. Lee, J. J. Lee, "Noncontact detection of ultrasonic waves using fiber optic Sagnac interferometer," IEEE Trans. Ultrason. Ferroelectr. Freq. Control **49**(6), 767–775 (2002).
22. E. Soczkiewicz, "The Penetration Depth of the Rayleigh Surface Waves," Nondestructive Testing and Evaluation **13**(2), 113–119 (1997).
23. J. D. Achenbach, *Wave Propagation in Elastic Solids*. 1984: Elsevier Science Ltd.
24. J. L. Rose, *Ultrasonic Waves in Solid Media*. 1999: Cambridge University Press.
25. I. Arias, and J. D. Achenbach, "Thermoelastic generation of ultrasound by line-focused laser irradiation," Int. J. Solids Struct. **40**(25), 6917–6935 (2003).
26. H. C. Wang, S. Fleming, and Y. C. Lee, "Simple, all-optical, noncontact, depth-selective, narrowband surface acoustic wave measurement system for evaluating the Rayleigh velocity of small samples or areas," Appl. Opt. **48**(8), 1444–1451 (2009).
27. D. Schneider, and T. Schwarz, "A photoacoustic method for characterising thin films," Surf. Coat. Tech. **91**(1–2), 136–146 (1997).
28. D. Schneider, T. Witke, T. Schwarz, B. Schoneich, and B. Schultrich, "Testing ultra-thin films by laser-acoustics," Surf. Coat. Tech. **126**(2–3), 136–141 (2000).
29. T. T. Wu, and Y. C. Chen, "Dispersion of laser generated surface waves in an epoxy-bonded layered medium," Ultrasonics **34**(8), 793–799 (1996).
30. A. Briggs, *Acoustic Microscopy*. 1992: Clarendon Press. Oxford.
31. H. C. Wang, S. Fleming, and Y. C. Lee, "A remote, non-destructive laser ultrasonic material evaluation system with simplified optical fibre interferometer detection," J. Nondestructive Evaluation **28**(2), 75–83 (2009).
32. J. Kushibiki, K. L. Ha, H. Kato, N. Chubachi, and F. Dunn, "*Application of Acoustic Microscopy to Dental Material Characterization*", IEEE 1987 Ultrasonics Symposium, pp.837–842, 1987.
33. S. D. Peck, J. M. Rowe, and G. A. Briggs, "Studies on sound and carious enamel with the quantitative acoustic microscope," J. Dent. Res. **68**(2), 107–112 (1989).
34. H. C. Wang, S. Fleming, S. Law, and T. Huang, *Selection of an appropriate laser wavelength for launching surface acoustic waves on tooth enamel*. in *Proceedings of IEEE Australian Conference on Optical Fibre Technology/Australian Optical Society (ACOFT/AOS)*. 2006. Melbourne, Australia.
35. R. G. Maev, L. A. Denisova, E. Y. Maeva, and A. A. Denissov, "New data on histology and physico-mechanical properties of human tooth tissue obtained with acoustic microscopy," Ultrasound Med. Biol. **28**(1), 131–136 (2002).
36. D. W. Blodgett, "Applications of laser-based ultrasonics to the characterization of the internal structure of teeth," J. Acoust. Soc. Am. **114**(1), 542–549 (2003).
37. N. Carlson, and J. Johnson, "Pulsed laser energy through fiberoptics for generation of ultrasound," J. Nondestructive Evaluation **12**(3), 187–192 (1993).

1. Introduction

Dental caries (tooth decay) is one of the most prevalent and costly diseases throughout the world. It is initiated by excessive mineral dissolution of the dental enamel caused by plaque bacteria induced acid [1,2]. Enamel is the semi-translucent outer layer of a tooth which envelops and protects the underlying dentin and it is the hardest and the most mineralised substance of the human body. Previous studies [3–5] have demonstrated that the level of mineralisation, hence the healthiness and strength, of dental enamel is linked to several of its mechanical properties, such as hardness and elastic modulus.

#111936 - $15.00 USD Received 9 Jun 2009; revised 28 Jul 2009; accepted 29 Jul 2009; published 19 Aug 2009

Currently, visual, tactile, and X-ray assessments remain the most common methods used for caries detection in a clinical setting [6]. They each have different advantages but are either destructive in nature or ineffective to detect caries at an early stage such that preventative therapies, such as enhanced remineralisation, can be applied instead of surgical interventions. In addition, all of these conventional techniques are unable to evaluate the level of enamel mineralisation. For dental research purposes, nano-indentation is widely used for measuring the elastic modulus of dental hard tissue [4,7]. Although it is able to make direct measurement, the indentation method is also destructive in nature and can only be applied to extracted teeth. In this regard, a localised and non-destructive technique that could potentially provide *in-vivo* evaluation of the elastic modulus of human dental enamel is desired.

Ultrasonic surface acoustic waves (SAW), also known as Rayleigh waves, have been widely utilised in the field of non-destructive evaluation (NDE) to characterise the elastic constants of surface materials and thin films [8–12]. In a complex inhomogeneous structure, such as a two-layer system, the wave is dispersed; its velocity varies with frequency. Determining the velocity at different frequencies yields a dispersion spectrum dependent on the elastic and geometric parameters of the material system. SAW velocity could thus be useful to evaluate the elastic constants of dental enamel and hence determine the state of the enamel mineralisation.

Conventional methods to generate and detect the SAW utilise contact transducers such as piezoelectric materials. These devices are well established but present several intrinsic limitations due to the manner of contacting and the requirement of a couplant to deliver ultrasound to and from the sample. For example, size limits spatial resolution and manoeuvrability; suitable couplants for sensitive materials are scarce; surface preparation is sometimes required; and the propagating SAW is susceptible to undesired influences from the transducer load and the wave energy leakage into the couplant layer, etc [13]. These drawbacks make the contacting methods impractical for measurements on human teeth.

Non-contacting methods that utilise laser and optical techniques to generate and measure elastic waves at a distance from the sample solve the problems mentioned above and offer additional advantages [13,14]. A laser beam can be focused onto small objects and provide better spatial resolution; and being non-contacting, the use of a laser eliminates the necessity for a couplant and the loading that could influence the wave propagation.

Generating SAW with optical methods is relatively straightforward; in our study we irradiate the sample surface with short-duration laser pulses focused into a thin line by a cylindrical lens. The setup can be simple, requiring one laser source, a few guiding mirrors and the focusing lens. The laser pulse energy can be maintained at a low level to ensure non-destructive thermo-elastic operation.

The optical detection mechanism in a remote NDE system is critical: the accuracy in extracting information from the typically nm or sub-nm amplitude elastic wave is important for the material constants determination [15,16]. Optical interferometry is a very sensitive way of measuring surface displacement. Michelson and other free space interferometers have been commonly utilised to measure elastic ultrasound but they have limited manoeuvrability and critical alignment of the optics can be tedious and inappropriate for many areas of practical deployment [13]. Optical fibre provides considerable practical advantages when used as the light steering medium of the interferometer, since no critical alignment of sensitive optics in the vicinity of the target is required [17]. Furthermore, the flexibility and miniature size of the optical fibre can improve the interferometer's capability to access areas that are difficult to examine with standard optics [18,19]. Different designs of optical fibre interferometer (OFI), such as Fabry-Perot [20] and Sagnac [21], have been demonstrated but they are cumbersome. In this study a simplified OFI that is easy to implement and control and is able to measure high-frequency ultrasound with minimum supporting components is described.

In this paper we present a laser ultrasonic system that consists of a cylindrical lens focused line-source for generation of broadband SAW impulses and a simplified design of OFI for detection of the elastic ultrasound. This system allows surface material evaluation through

#111936 - $15.00 USD Received 9 Jun 2009; revised 28 Jul 2009; accepted 29 Jul 2009; published 19 Aug 2009

SAW dispersion analysis and its performance and reliability will be first demonstrated on various metal structures. We then focus on the novel combination of these techniques to provide evaluation on localised areas of extracted human tooth surface. For the first time, to the best of our knowledge, qualitative evaluation of sound enamel using such a system is presented. The results obtained demonstrate the potential of this optical NDE technique for future *in-vivo* tests.

2. Laser ultrasonic NDE technique

2.1 Acoustic theory

The wave energy of a SAW, and hence the wave motion, is concentrated within a penetration depth of the order of its wavelength, λ, beyond which the wave amplitude quickly becomes negligible [22]. This essentially means that the SAW velocity, c_R, is governed by the elastic constants of the material depth it probes. In common with all wave motions, the SAW velocity is equal to the product of its wavelength and frequency, and hence the SAW penetration depth, z, can be estimated from the relation:

$$z \approx \lambda = c_R / f, \tag{1}$$

where f is the signal frequency.

In an isotropic homogeneous medium, c_R is independent of the signal frequency as well as propagation direction and given by the approximated relation [23]:

$$c_R \approx \frac{0.87+1.12\nu}{1+\nu}\sqrt{\frac{E}{2\rho(1+\nu)}}, \tag{2}$$

where E is the elastic modulus, ρ is density and ν is the Poisson's ratio.

For a multilayer medium of different elastic properties, the wave propagation is influenced by all the layers it probes such that c_R is governed by a generalised dispersion Eq. (24). To understand the dispersion effect, consider a broadband surface wave propagating in the x_1 direction on a sample consisting of a substrate coated with an upper layer that has a lower SAW velocity, as shown in Fig. 1. Such a medium is of direct interest to our study since human tooth can be considered as a two-layer system within the scope of our intended investigation.

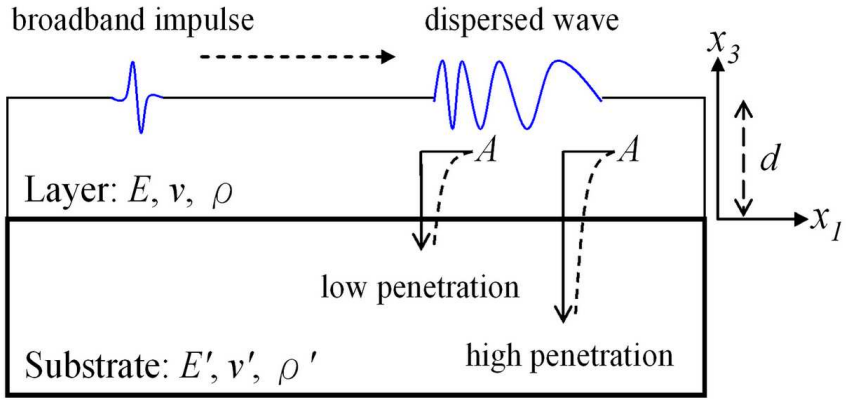

Fig. 1. Surface wave dispersion in a two-layer system.

A broadband SAW impulse can be regarded as the superposition of surface waves with different frequencies. Referring to Fig. 1, the amplitude, A, of the SAW motion depends on the frequency. The higher frequency components are more influenced by the layer, travelling with a relatively slower velocity whereas the lower frequency components are influenced

#111936 - $15.00 USD Received 9 Jun 2009; revised 28 Jul 2009; accepted 29 Jul 2009; published 19 Aug 2009

more by the substrate elastic parameters. Thus the phase velocity c_R becomes a function of frequency and the SAW impulse is dispersed as it propagates along its path.

Figure 1 shows an example of the normal dispersion where the velocity reduces as the signal frequency increases. The opposite situation, where the wave velocity increases with increasing frequency, is known as anomalous dispersion. In both cases, the dispersed waveform contains the desired information about the material system.

2.2 System configuration

The schematic of the Laser NDE system for SAW dispersion measurement on samples of different dimension and form is illustrated in Fig. 2.

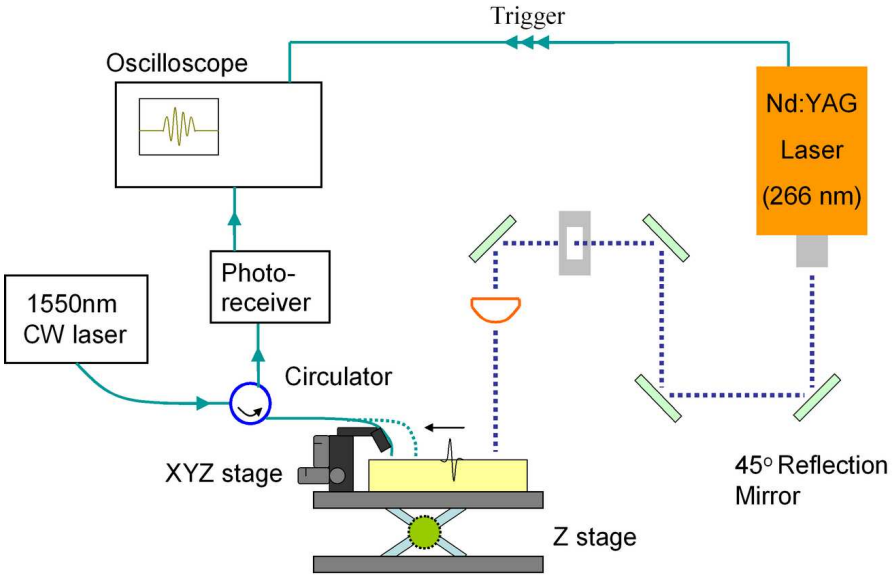

Fig. 2. Arrangement of the laser NDE system and the SAW dispersion measurement.

A solid state Nd:YAG laser (LOTIS TII LS-2137U), operating on the fourth harmonic at 266 nm, was used to excite the surface wave. The source laser pulses, with ~5 ns duration under Q-switched mode, were directed by several mirrors through a rectangular mask and focused into a thin line by a cylindrical lens onto the sample surface (shown on the right of Fig. 2). A line-source generated SAW propagates perpendicular to the line-source and experiences less attenuation than a point-source produced signal.

The generated surface wave is narrow in both temporal and spatial domains, it contains a wide frequency bandwidth enabling the signal to probe multiple layers in the material simultaneously, which is desired for the SAW dispersion measurement. The temporal and spatial profiles of the SAW impulse are predominately influenced by the laser pulse duration and the width of the line-source: the generated signal becomes broader and its magnitude decreases as the laser line-source is spread out in space and time [25].

In our measurement setup, different samples were placed on a manual Z-stage for adjusting the separation between the lens and the sample and hence the line-source width (defocusing the image). Reducing the line width can increase the signal bandwidth but this inevitably raises the irradiating power density and may damage the specimen surface. Throughout the measurements the length of the line-source remained constant around 1.6 mm and the line width varied between 60~100 μm (recorded on a thermally sensitive paper and measured under an optical microscope). The laser repetition rate was set to 1 Hz and the average pulse energy was 0.1~0.3 mJ, measured after the mask with an optical power-meter. This gives a maximum power density of 6.25×10^7 Wcm^{-2}, which is close to the damage threshold for metals [13]. However, the actual absorbed laser power is less as a result of

#111936 - $15.00 USD Received 9 Jun 2009; revised 28 Jul 2009; accepted 29 Jul 2009; published 19 Aug 2009

reflection and scattering. During measurements the laser pulse energy and the sample surface were constantly monitored to ensure that no physical damage, such as ablation and melting, occurs.

Detection of the ultrasound was performed by the OFI (shown on the left of Fig. 2) consisting of a 1550 nm continuous-wave laser (Photonics TUNICS-Plus) as the light source, a 3-port optical fibre circulator (Nortel Networks HRC-1550-Q3-1010) and a photo-receiver (New Focus 1611 1 GHz). These three components were joined using fibre connectors. The detected signal was averaged 32 times and displayed on a digital oscilloscope (Tektronix TDS5104B) with a trigger signal from the Nd:YAG laser.

The tip of the middle port fibre of the circulator was cleaved to act as the probe head and placed on a micron-precision three axis (XYZ) positioning-stage so its distance to the sample surface can be adjusted to optimise the returning signal strength and the spatial resolution, as well as making measurements at different locations. This positioning-stage permits measurements between 1 mm and 12 mm from the line-source, with 0.01 mm precision.

The basic principle of this OFI is similar to a reference beam interferometer. The coherent laser light from the source, I_0, was coupled into the circulator. As it reaches the middle port (sensing tip), about 4% of the light will be internally (Fresnel) reflected at the silica/air interface and serves as the reference beam, I_1. The rest of the light is incident on the sample surface and then reflection causes a small portion of it, I_2, to be coupled back into the fibre and become the measurement beam. Throughout the rest of the system, I_1 and I_2 co-propagate toward the third port and this essentially common path environment means that the path difference of the two beams, and hence their relative phase, depends only on the separation between the fibre tip and the sample surface. In a typical ultrasonic measurement the phase modulation is less than π, which means that the elastic wave vibration amplitude is less than a quarter of the OFI source wavelength, and the interference intensity becomes a very good measure of the absolute acoustic waveform. However, the measured interference signal does not contain information about the absolute ultrasonic wave amplitude since we did not have the means to know precisely the initial static phase difference (equivalent to controlling the probe-to-sample separation on a nanometre scale).

Some critical characteristics of the OFI include the following. The bandwidth of the detection system is limited by the response time of the photoreceiver, which is 1 GHz, sufficient for most ultrasonic measurement. The spatial resolution of the OFI predominately depends on the measurement beam size, which is affected by the fibre core parameters as well as the probe-to-sample separation. Consider Fig. 3, the light that emanates from the fibre core is diverging and thus the area illuminated on the sample surface increases with the probe-to-sample separation. Large probe-to-sample separation is undesirable since the illuminating beam size can be larger than one cycle of the ultrasonic wavelength, which causes I_2 to contain averaged information of the propagating waveform and low spatial resolution. In addition, at large probe-to-sample separation the amount of the reflected light captured by the fibre is minimised, that means that the magnitude of I_2 is small compared to I_1 which results in poor interference intensity contrast.

#111936 - $15.00 USD Received 9 Jun 2009; revised 28 Jul 2009; accepted 29 Jul 2009; published 19 Aug 2009

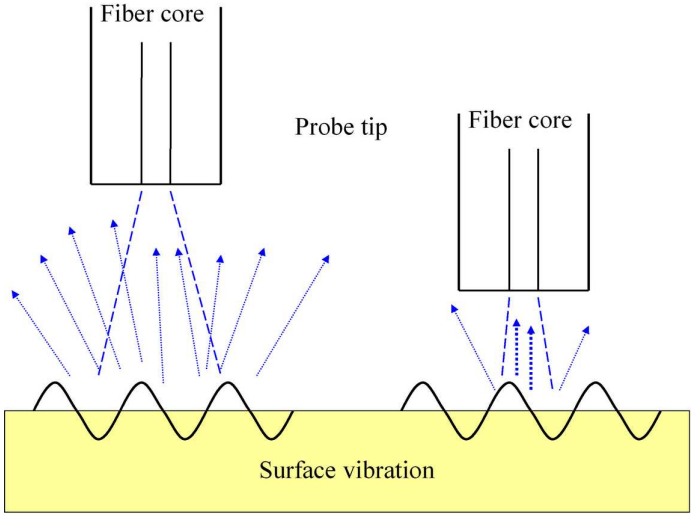

Fig. 3. Comparison between large and small probe-to-sample separation.

When the probe tip is placed close to the sample, the measurement beam size is more confined, allowing more light to be coupled back into the fibre and hence increase the interference contrast. In the typical measurement conditions, the light gathered back into the optical fibre, I_2, is formed predominately by the reflection off a small area directly beneath the fibre centre. This means that the actual measurement beam size (not the illuminated beam size) is similar to the fibre core. For the standard single mode fibre used, the core diameter is typically <10 μm which is small compared to the ultrasonic wavelength in our experiments, and thus there is negligible averaging effect allowing truly point to point measurements. All measurements were made with a probe-to-sample separation of 5 mm or smaller. Initial performance of the OFI can be found in previous publications [26].

2.3 Determination of the experimental dispersion spectrum

To determine the experimental dispersion curve, the generated surface waves were measured at various locations along the epicentral axis of the line-source. The recorded wave signals were digitally bandpass filtered (1 to 50 MHz) to reduce the low and high frequency noise. Two signals, at locations x_1 and x_2, were selected for dispersion analysis. They were cross-correlated in order to identify and exclude the noise signals, and then Fourier transformed. The phase difference between the ultrasonic signals, $\varphi(f)$, was determined from the phase angle of the Fourier spectrum. Inserting these into Eq. (3) yields the frequency dependent phase velocity and hence the experimental dispersion curve:

$$c(f) = 2\pi f \frac{x_2 - x_1}{\varphi(f)}. \tag{3}$$

A cross-power spectrum, which is the magnitude of the Fourier spectrum, can be used to identify the usable frequency range with sufficient signal-to-noise ratio [27]. The reliable bandwidth was determined experimentally and we set the cut-off frequency when signal has dropped substantially, or permanently, below –20 dB level of the cross-power spectrum (this is demonstrated later with the experimental results). Outside this range the uncertainty of the dispersion curve increases drastically. The accuracy of the phase velocities at the low frequency region depends on the spacing of the measurement positions, the larger the separation the less the uncertainty will be [28,29]. Furthermore, the lower limit of the useable band was chosen to be around 1 MHz as signals of lower frequencies contain less information about the surface and suffer from low frequency ambient noise.

#111936 - $15.00 USD Received 9 Jun 2009; revised 28 Jul 2009; accepted 29 Jul 2009; published 19 Aug 2009

2.4 Validation measurements on common metals

Prior to applying this system for evaluating human dental enamel, the feasibility and accuracy of our system for measuring different types of surface waves (both non-dispersed and dispersed) was investigated. In addition, the reliability of the analysis technique for determining the experimental SAW dispersion spectrum must be tested by correlating with theoretical expectations. In this section we present the application of our NDE system to different structures made of common metals and demonstrate that the system is able to provide remote, non-destructive and reliable surface layer evaluation on a small localised area.

Homogeneous isotropic materials namely aluminium and brass blocks with known Rayleigh velocities were used (aluminium ~2950 ms^{-1}, brass ~1970 ms^{-1} [30]). Figure 4 shows the Rayleigh waves on the aluminium sample measured at various locations between 2 mm and 10 mm from the line source with 1 mm step size. Note the wave amplitudes are normalised (such that the peak amplitudes are the same and the traces do not overlap) and the y-axis is not the scale of the traces but rather it serves only as a label to indicate for each trace the relevant location from the line-source. No waveform broadening indicates that no dispersion occurs in this homogeneous medium.

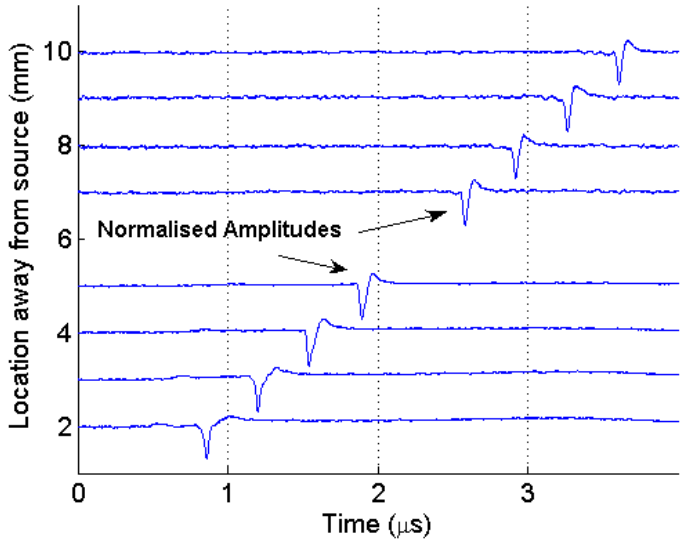

Fig. 4. Rayleigh waves on the aluminium sample measured at different locations away from the source. [N.B.: the traces are identically scaled arbitrary units, see text for details.]

Two signals, measured on aluminium at 2 mm and 10 mm away from source, were chosen and analysed according to the procedure discussed above. The surface wave phase velocity as a function of frequency was calculated using Eq. (2) and is displayed in Fig. 5. The same measurement was performed on the brass block and the determined velocity is plotted also on Fig. 5.

The signal-to-noise ratios for these sets of measurements were very high, such that the usable band extends to 30 MHz (demonstrated by the expected stable velocity value). Perturbations can be observed in the <1 MHz region, indicated by the dashed line in Fig. 5, as discussed above and should be ignored.

#111936 - $15.00 USD Received 9 Jun 2009; revised 28 Jul 2009; accepted 29 Jul 2009; published 19 Aug 2009

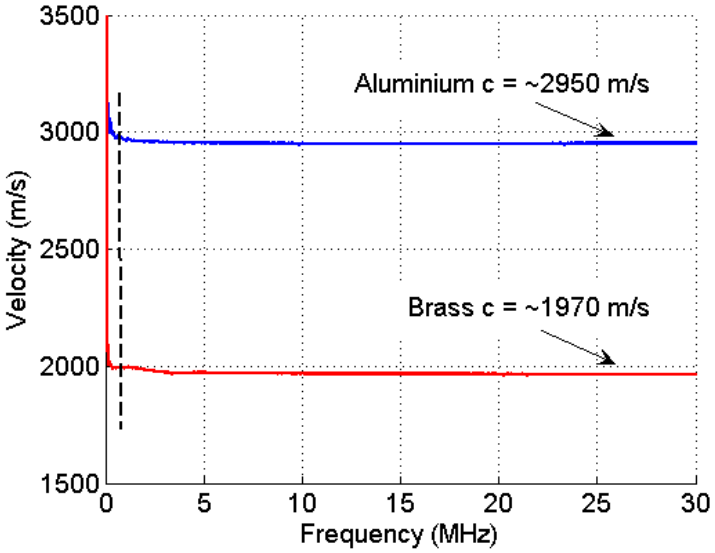

Fig. 5. Experimental Rayleigh phase velocities for aluminium and brass sample.

These experimental results for both homogeneous block materials match very well with the theoretical values (less than 1% difference) and they demonstrate, as expected, that no dispersion occurred in these uniform media.

For the study of a dispersive two-layer system, a sample composed of a ~40 μm thick nickel film sputtered onto a thick fused quartz glass substrate was used. The SAW velocities of the materials were known (nickel: c_R ~2700 ms^{-1} glass: c_R ~3400 ms^{-1}). Figure 6 shows the Rayleigh waves measured along the propagation path up to 6 mm away from the line-source with 1 mm spacing. The distortion of the acoustic waveform is apparent and in this case it is obvious that the low frequency components, more influenced by the glass substrate, travel faster. This indicates that the expected normal dispersion takes place in this system.

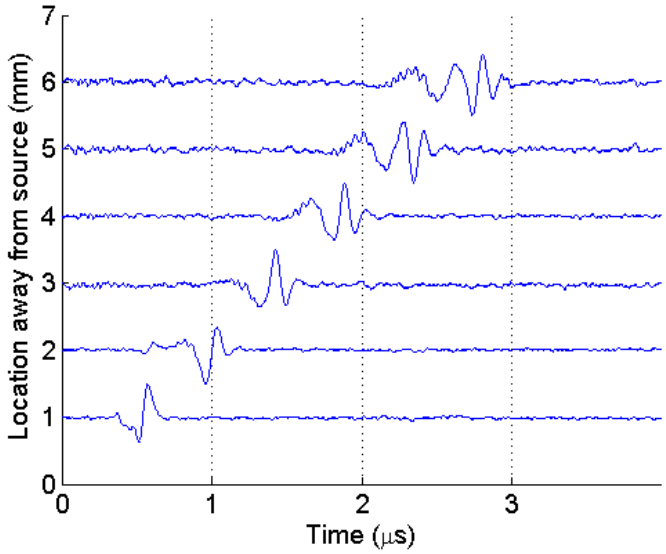

Fig. 6. Surface waves on a two-layer system of Ni film on glass substrate measured at locations 1 mm to 6 mm away from the source. [N.B.: Y-axis as per Fig. 4.]

#111936 - $15.00 USD Received 9 Jun 2009; revised 28 Jul 2009; accepted 29 Jul 2009; published 19 Aug 2009

Signals with the furthest separation were once again chosen and cross-correlated for the dispersion analysis. The cross-power spectrum between the two signals is displayed in Fig. 7 from which we determined the upper limit of the useable spectral band to be around 20 MHz. The lower limit was again chosen to be 1 MHz for reasons mentioned above.

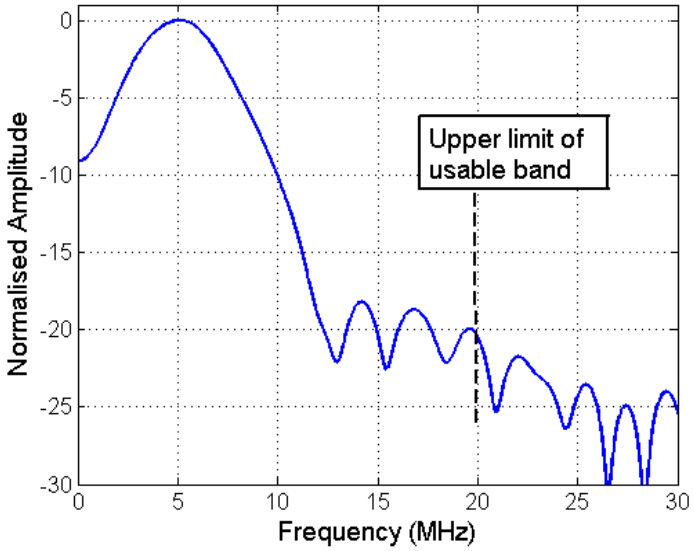

Fig. 7. Cross-power spectrum between signals measured at 1 mm and 6 mm from the source. The usable bandwidth spanned ~20 MHz.

The experimental dispersion curve is plotted in Fig. 8. Within the reliable bandwidth, indicated by the dashed lines, the shape of the curve matches well with the qualitative expectation of the interaction between the ultrasound and the physical structure: the low frequency components travel with a velocity close to that of the glass and gradually decreases as the wave becomes more influenced by the nickel film at higher frequencies.

To confirm the thickness of the nickel film, and hence the accuracy of the experimental result, the partial wave technique presented in [24] was used to calculate the theoretical SAW dispersion spectrum using known parameters of the two substances with different film thicknesses (30 μm, 40 μm and 50 μm). The theoretical spectra were also plotted and displayed in Fig. 8. The experimental curve clearly fits best with the 40 μm simulation within the usable bandwidth and beyond this the experimental results diverge from the theoretical prediction. The actual thickness of the nickel film was then measured with an optical micrometer and found to be 42 ± 2 μm (it was not a perfectly uniform film). This technique can also be used inversely to determine the elastic modulus of the surface layer if the thickness is known.

#111936 - $15.00 USD Received 9 Jun 2009; revised 28 Jul 2009; accepted 29 Jul 2009; published 19 Aug 2009

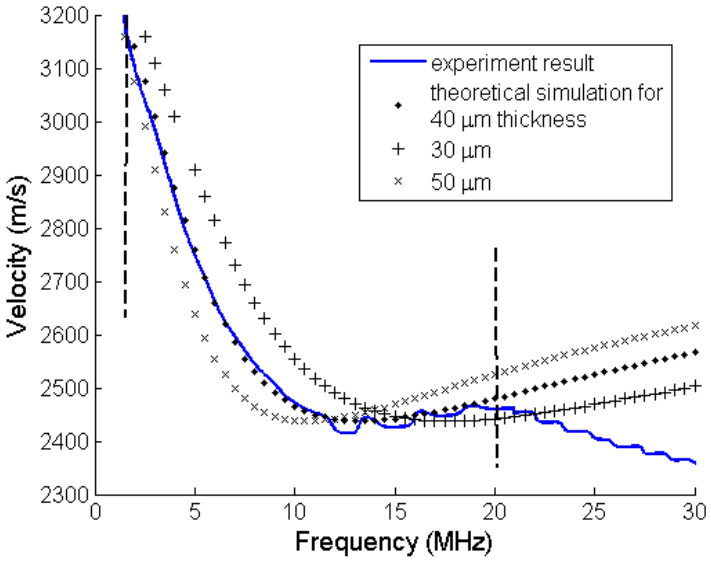

Fig. 8. Experimental and theoretical dispersion curves for nickel film on glass substrate.

The above measurements demonstrate that our optical NDE system can generate and detect different types of surface waves on various samples. Excellent matches were obtained in fitting the experimental dispersion curves with theoretical simulations. This demonstrates that the curvature and the trend of the experimental dispersion curve within the reliable bandwidth are accurate in terms of revealing the state of elasticity of the medium in which the SAW propagates, most importantly the elastic strength as a function of depth. The main source of uncertainty in this technique will most likely be the error in measuring the signal separations from the OFI translation stage manual micrometer adjustment. More extensive testing of this system on a wider variety of samples further demonstrated its accuracy and reliability [31].

3. Evaluation of human dental enamel

3.1 Acoustic properties of human enamel

The unevenly distributed composition and the highly oriented microstructure of tooth enamel result in anisotropic and inhomogeneous mechanical and elastic properties [4]. Kushibiki et al. [32] used line-focused-beam scanning acoustic microscopy (SAM) and measured the Rayleigh wave velocity as a function of propagation direction on the labial surface of extracted human incisors and observed that the velocity values vary between about 3105 ms^{-1} to 3155 ms^{-1} with the maximum obtained in the direction parallel to the tooth axis (direction from the crown to root). Peck and colleagues [33] repeated the investigation on the surface of human permanent molars using SAM and reported that the Rayleigh velocity varied between about 3075 ms^{-1} to 3142 ms^{-1} with the maximum velocity also in the direction parallel to the tooth axis. The SAM technique has drawbacks in that the measuring steps can be tedious and lead to prolonged time required. Also special polishing procedures for the specimens are pre-requisite which makes the technique ill-suited for clinical applications. In addition, it requires coupling fluid and its physical conditions (e.g. temperature) need constant monitoring and maintaining.

3.2 Safety and Efficiency Consideration

Launching a SAW efficiently and non-destructively using a laser on the surface of tooth enamel is essential for the remote NDE technique to be applicable in dentistry. A study of

#111936 - $15.00 USD Received 9 Jun 2009; revised 28 Jul 2009; accepted 29 Jul 2009; published 19 Aug 2009

laser wavelength absorption by human enamel [34] found that UV light (~300 nm) was better absorbed than near-IR light, with an absorption coefficient of 4045 ± 200 m^{-1} and the corresponding penetration depth of 0.26 ± 0.01 mm. The shallow penetration depth means that the surface wave generation will be efficient and hence for the enamel measurement we chose the 266 nm emission from the Nd:YAG laser to be SAW source.

In addition, the laser damage threshold for enamel at 266 nm was experimentally estimated. We used a tooth sample and irradiated it with a line-source of laser pulse energy at ~1 mJ and focused the line-source gradually until thermal damage (predominately ablation) started to occur on the enamel surface. The corresponding line-source dimension was measured to be ~1.4 mm by ~0.02 mm which gives a power density of ~7.5×10^8 Wcm^{-2}. For our measurements on human dental enamel, presented below, we operated at a power density value that is below this estimated threshold with a margin such that all our experiments are non-destructive.

3.3 Measurements and results

Among the various teeth, it is advantageous to choose the incisor for initial studies because its front or labial surface has the largest flat area of enamel. In addition, the enamel thickness is relatively constant (~1 mm) over a wide region near the centre of the incisor front surface. This is desirable because the measured SAW dispersion will not depend significantly on the uneven thickness of the enamel layer but rather on the elasticity variation. Two recently extracted human incisors were selected for the measurements (labelled A and B). Thin layers from the backs of the teeth were removed with a diamond blade such that the sample can be placed on the measurement holder (on the Z-stage). The front surfaces of the two samples were not modified.

The line-source measurement setup and the procedures were the same as described above. Figure 9 shows a photograph taken during the actual measurement of sample A, where the position of the line-source is indicated by the fluorescence from the UV irradiation line-source. In this study we intended to avoid the effects of anisotropy in the enamel and made measurements only along the tooth axis. The recordings of the Rayleigh waves were made at several positions along the propagation path (perpendicular to the line-source epicentre). Both samples were measured ten times and in each measurement we shifted the sample position randomly by a small amount (± 0.2 mm) in the direction perpendicular to the propagation path, such that the evaluation results will be the averaged contribution from an area of rectangular shape with ~0.4 mm width.

#111936 - $15.00 USD Received 9 Jun 2009; revised 28 Jul 2009; accepted 29 Jul 2009; published 19 Aug 2009

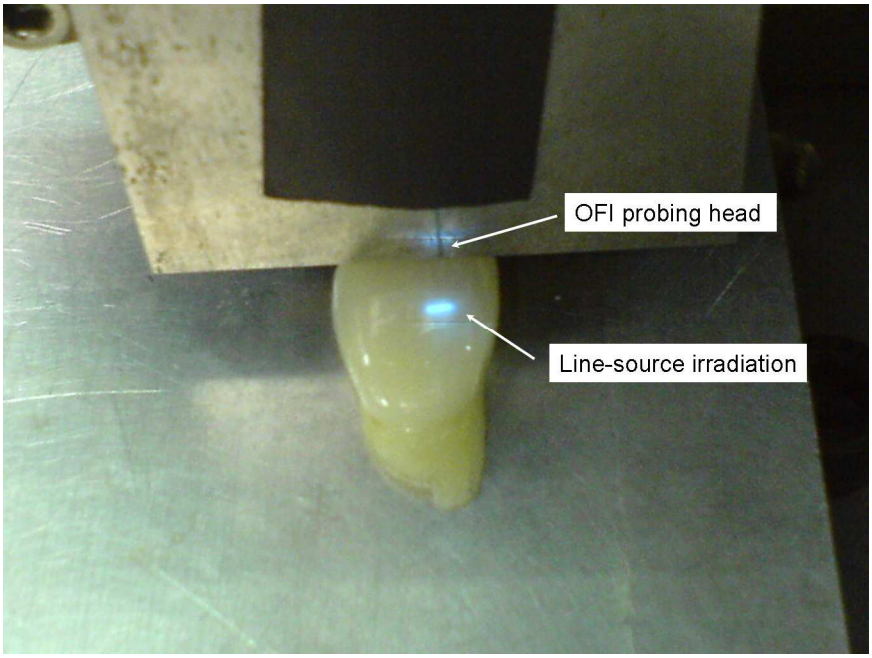

Fig. 9. The front surface of incisor A was irradiated with the line-source and the OFI detection tip was placed a few mm away.

Typical recorded wave signals, from both sets of measurements, at various locations away from the line-source are presented in Fig. 10. The temporal shape of the Rayleigh waves appeared to be consistent during propagation.

#111936 - $15.00 USD Received 9 Jun 2009; revised 28 Jul 2009; accepted 29 Jul 2009; published 19 Aug 2009

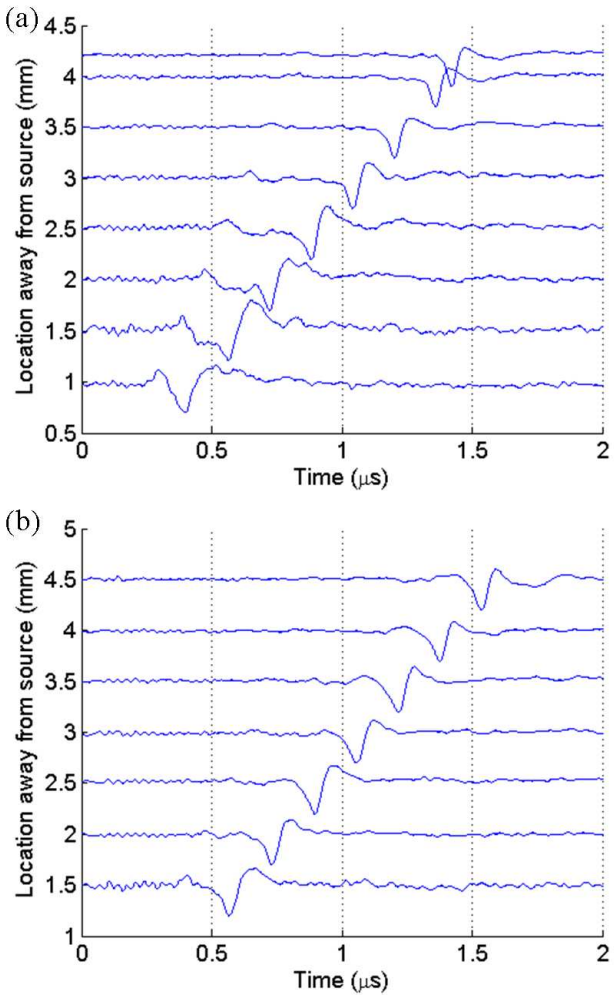

Fig. 10. Rayleigh waves recorded at different locations from the line-source on the front surface of (a) sample A and (b) sample B. [N.B. Y-axis as per Fig. 4.]

Two signals, with a separation of more than 2 mm, were selected from each measurement for the dispersion analysis. The dispersion analysis was performed in accord with the procedure discussed previously. The cross power spectrum again serves as the indication of the signal strength and the upper limit of the reliable bandwidth (R.B.). A typical cross power spectrum from the sample A measurements is shown in Fig. 11, from which we estimated that the R.B. is within 1 ~21 MHz. The R.B. for the sample B measurements was very similar to this value.

#111936 - $15.00 USD Received 9 Jun 2009; revised 28 Jul 2009; accepted 29 Jul 2009; published 19 Aug 2009

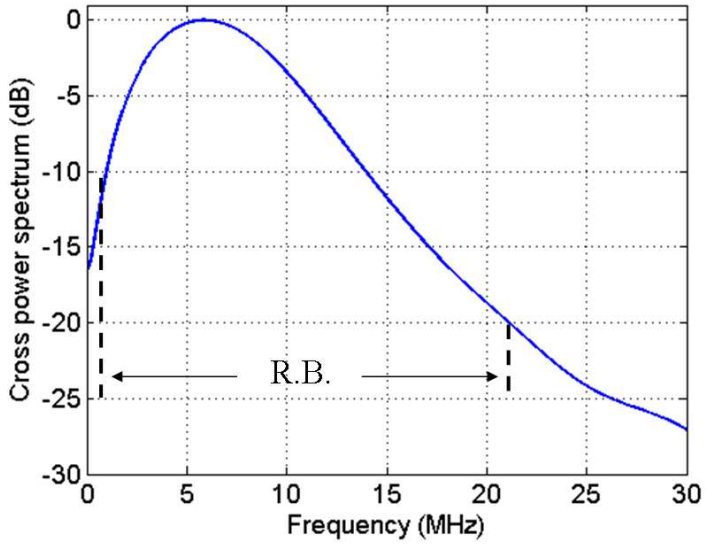

Fig. 11. Cross power spectra from one of the sample A measurements.

Dispersion spectra were calculated and for each sample the ten-times-averaged value was used as the final result and presented in Fig. 12 with standard deviation error-bars. In both samples the SAW velocities begin at a low value (~2900 ms^{-1}) at 1 MHz and gradually increase with frequency and reaches a value of ~3150 ms^{-1} at ~6 MHz and remain relatively constant thereafter. This value is very close to that previously reported [32,33].

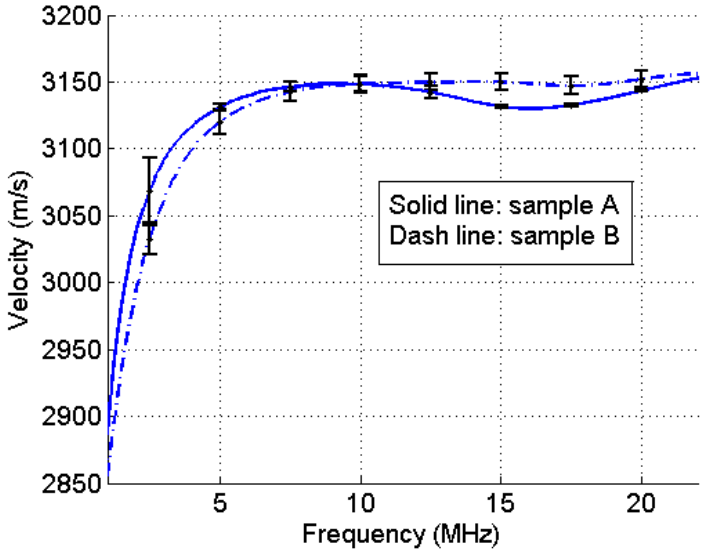

Fig. 12. Dispersion curves of the final averaged results from sample A and B.

The observation in the low frequency region can be explained by the influence of dentin, which has a much lower Rayleigh velocity than enamel [35,36]. For Rayleigh waves travelling at ~3150 ms^{-1} with frequencies of 1 ~6 MHz, the corresponding probing depths are estimated using Eq. (1) to be 3.15 ~0.53 mm. Since the enamel is typically 1 mm thick, the propagation structure for these low frequency Rayleigh wave components can be considered

#111936 - $15.00 USD Received 9 Jun 2009; revised 28 Jul 2009; accepted 29 Jul 2009; published 19 Aug 2009

as a two-layer system (sound bulk enamel on top of dentin). Anomalous dispersion (velocity rise with frequency) is hence expected from the significant influence of the lower elastic modulus dentin. Once the Rayleigh wave penetration depth is below a certain value (in this case ~0.5 mm at ~6 MHz) at which the influence of dentin becomes negligible, the Rayleigh wave propagates and probes only the enamel as a one layer system. The Rayleigh velocity remain approximately constant at ~3150 ms^{-1} which means that inside sound enamel the elastic values don't change significantly with depth.

The dispersion curve profiles and the SAW velocity values within the reliable bandwidth are consistent in both individual human incisors, which suggest that the elasticity, and hence the mineralisation, are similar. In addition, these results are very promising as they match physical expectations regarding the propagation of the Rayleigh wave on the human teeth. This is the first time that the state of elasticity (mineralisation) of human dental enamel has been evaluated using the laser SAW dispersion method.

4. Conclusion

In this paper we presented a remote laser ultrasonic NDE system that consists of a laser line-source for generating broadband surface acoustic waves and an optical fibre interferometer for detecting the ultrasound. The novel combination of these techniques provides important new functionality for non-destructive surface material evaluation of samples with small dimensions. The measurement system was easy to implement and operate and a typical test can be very time efficient, requiring only two signals for the dispersion analysis.

Results from measuring common metal structures demonstrated the capability of this NDE system for measuring non-dispersed Rayleigh waves on homogeneous media as well as dispersed surface waves on a two-layer system. The experimental dispersion curves were determined and they fit well with theoretical values, which confirmed the accuracy of our NDE technique.

We applied this NDE technique and evaluated the elasticity of extracted human teeth, for the first time, and obtained very promising results. The measurements on these small samples were made possible due to the utilisation of the fibre interferometer. The characteristics of the experimental dispersion curves match well with physical expectations. The influence of dentin was observed by the anomalous dispersion (increase in velocity with frequency) in the low frequency spectrum. The SAW velocity value of the sound enamel matched well with previous studies.

At the current stage, whilst this laser NDE system has been demonstrated to be in principle suitable for *in-vivo* measurements, there are a few straightforward developments which would be needed to permit *in-vivo* testing. First, optical fibre guided generation of SAW using short pulsed fibre lasers can be utilised to provide better manoeuvrability over standard optics [37], and hence improve the accessibility for enamel measurement. Second, a hand-held device which combines the generation and detection fibres together in a single probe could be assembled. This can ultimately serve as the probing tool for *in-vivo* measurements. Third, higher frequency SAW can be readily generated by using a laser source of shorter duration, which would improve the range of usable frequency band.

The current optical NDE system can be further utilised to study human dental enamel with different state of elasticity, for example, measuring decayed enamel.

Acknowledgement

This work was funded by the Australian Government and Bio-Dental Technology Pty. Ltd. under an ARC Linkage Grant, No. LP0561184.

#111936 - $15.00 USD Received 9 Jun 2009; revised 28 Jul 2009; accepted 29 Jul 2009; published 19 Aug 2009